Some specificities of wetting by cyanobiphenyl liquid crystals

2009 J. Phys.: Condens. Matter 21 464129

(http://iopscience.iop.org/0953-8984/21/46/464129)

IOP PUBLISHING JOURNAL OF PHYSICS: CONDENSED MATTER

J. Phys.: Condens. Matter **21** (2009) 464129 (11pp) doi:10.1088/0953-8984/21/46/464129

Some specificities of wetting by cyanobiphenyl liquid crystals

U Delabre, C Richard and A M Cazabat

Laboratoire de Physique Statistique, Ecole Normale Supérieure, Université Pierre et Marie Curie, CNRS, 24 rue Lhomond, 75231 Paris Cedex 05, France

E-mail: cazabat@lps.ens.fr

Received 20 May 2009, in final form 18 August 2009
Published 29 October 2009
Online at stacks.iop.org/JPhysCM/21/464129

Abstract

The present paper provides an up to date restatement of the wetting behaviour of the series of cyanobiphenyl liquid crystals (LCs) on usual substrates, i.e. oxidized silicon wafers, water and glycerol, at both the macroscopic and microscopic scale, in the nematic range of temperature. We show that on water the systems are close to a wetting transition, especially 5CB and 7CB. In that case, the wetting behaviour is controlled by the presence of impurities. On a mesoscopic scale, we observe for all our (thin LC film–substrate) systems an identical, complex, but well defined general scenario, not accounted for by the available models. In the last part, we present a study on line tension which results from the specific organization of LCs at the edge of the nematic film. We report preliminary results on two-dimensional film coalescence where this line tension plays a major role.

(Some figures in this article are in colour only in the electronic version)

1. Introduction

The present paper provides an up to date restatement of the wetting behaviour of the series of cyanobiphenyl (*n*CB) liquid crystals (LCs) on usual substrates, i.e. oxidized silicon wafers, water and glycerol, at both the macroscopic and microscopic scale. Published data on the properties of the *n*CB series have been collected. Our previous experimental studies on the wetting behaviour of standard 5CB, 6CB and 8CB samples have been complemented by new experiments using standard 7CB and pure 5CB and 8CB, and also by film pressure measurements of the various compounds both on water and on glycerol.

The paper is organized as follows.

- In the first part, contradictory observations on the wetting behaviour on water, and quite scattered values of surface tension data of the *n*CB, are reported in the literature. We show that the scattering of the data is due to the presence of surface active impurities in the standard LC samples. We also show that on water the systems are close to a wetting transition, especially 5CB and 7CB. In this case, the wetting behaviour is controlled by the presence of impurities.
- In the second part, the structure of thin LC films is presented. We show that this is still an open problem, and so are the contributions to the surface free energy of flat, extended films. Our approach is to accumulate experimental data on an (LC–substrate) series in a wide range of length scales. We observe for all series an identical, complex, but well defined general scenario, not accounted for by the available models. There are also local intriguing differences between the series. The aim of the second part of the paper is to report the main features of the general scenario, in order to provide a basis for further theoretical analysis. The local specificities will more probably require a molecular modelling.
- In the third part of the paper, another contribution to the free energy is considered. A measurable line tension results from the specific organization of LCs at the edge of the nematic film. We report preliminary results on two-dimensional film coalescence where this line tension plays a major role. Such a situation differs from the already known 2D or 3D coalescence processes. We identify the leading terms in both the early and late steps of this 2D coalescence.

In most studies and applications, liquid crystal (LC) samples are bounded by two solid plates and wettability by the liquid is not a relevant parameter. Questions about wettability arise in the more academic case of LC films deposited on

a substrate. Then, the scattering of the experimental data for surface or interfacial tensions suggests that the answer is probably not straightforward [1–10].

The specificity of LC is that the structure of the film, and therefore the contributions to the free energy, depend on its thickness. This is a case where scales must be clearly separated.

- Wettability refers to thermodynamic equilibrium and macroscopic scale. In principle it is characterized by a combination of interfacial tensions. We present the example of benzene on water to emphasize that (i) thermodynamic equilibrium may be slow, (ii) in the non-wetting case, the film in equilibrium with the bulk phase deserves a specific analysis.
- The microscopic scale contains information on the contributions to the free energy. Ellipsometric studies of slowly spreading microdroplets, or analysis of thin films deposited on the substrates, are convenient tools to investigate the LCs out of equilibrium with the bulk phase.

The wettability of a substrate S by a liquid L under inert atmosphere A is characterized by the spreading parameter S [11–14], $S = \gamma_{SA} - \gamma_{LA} - \gamma_{LS}$.

The interfacial tensions γ_{ij} are considered at thermodynamic equilibrium, i.e. $S \leqslant 0$. For dynamic situations, the relevant quantity is the initial spreading parameter S_0, defined using the short time values $\gamma_{(ij)0}$ of the interfacial tensions. In the present discussion, we neglect the volatility of the liquids, LCs, water or glycerol, therefore the gas phase plays no role. However, S and S_0 may significantly differ, as for benzene on a water substrate [12], which is a good introduction to LC films. As for many low surface tension liquids, benzene first spreads on water:

$$\gamma_{(\text{water/air})0} = 72.8 \times 10^{-3}\ \text{N m}^{-1},$$

$$\gamma_{(\text{benzene/air})0} = 28.9 \times 10^{-3}\ \text{N m}^{-1},$$

$$\gamma_{\text{benzene/water}} \approx 35 \times 10^{-3}\ \text{N m}^{-1}$$

$$S_0 \approx 72.8 - (28.9 + 35) \approx +8.9 \times 10^{-3}\ \text{N m}^{-1} > 0.$$

Then it retracts, and the equilibrium situation is a thin benzene film [12] in contact with a macroscopic benzene lens collecting the rest of the liquid[1].

$$\gamma_{(\text{saturated water+benzene film})/\text{air}} \cong 62.2 \times 10^{-3}\ \text{N m}^{-1},$$

$$\gamma_{\text{saturated benzene/air}} = 28.8 \times 10^{-3}\ \text{N m}^{-1}$$

$$S \approx 62.2 - (28.8 + 35) \approx -1.6 \times 10^{-3}\ \text{N m}^{-1} < 0.$$

S is negative and close to zero; i.e., the contact angle of the macroscopic benzene lens is very small. The thin benzene film on water has a film pressure

$$\pi = \gamma_{(\text{water/air})0} - \gamma_{(\text{saturated water+benzene film})/\text{air}} \cong 72.8 - 62.2 \cong 10.6 \times 10^{-3}\ \text{N m}^{-1}.$$

[1] The surface tension of benzene is practically unchanged when saturated in water.

This thin film of benzene is a part of the air–water interface at equilibrium with the macroscopic reservoir of benzene. As emphasized by several authors [12], it is probably a multilayer. We must keep in mind this scenario when analysing the behaviour of LC films.

2. Macroscopic wetting behaviour of cyanobiphenyls

2.1. Materials

The LCs investigated are three members of the cyanobiphenyl series, 5CB, 6CB and 8CB, from Sigma-Aldrich (purity 98%, referred to as 'standard' in the following) used as received. More recently, we made some checks with the 7CB, and also with two higher purity samples (>99%, 5CB and 8CB from Alfa Aesar). The transition temperatures are

$T_{\text{solid–nematic}} = T_{SN} = 24\,^{\circ}\text{C}$ for 5CB,
14.5 °C for 6CB, 30 °C for 7CB

$T_{\text{solid–smectic}} = T_{SSm} = 21.5\,^{\circ}\text{C}$ for 8CB

$T_{\text{smectic–nematic}} = T_{SmN} = 33.5\,^{\circ}\text{C}$ for 8CB

$T_{\text{nematic–isotropic}} = T_{NI} = 35.3\,^{\circ}\text{C}$ for 5CB, 29 °C for 6CB,
42.8 °C for 7CB, 40.5 °C for 8CB.

5CB has been studied at room temperature, i.e. 22 ± 1 °C, far from the NI transition, 6CB, 7CB and 8CB in the whole nematic range. In fact, surface-induced melting is the rule, and nematic films persist even if the system is cooled below the T_{SN} temperature.

The liquid substrates are pure water (18.2 MΩ cm) and glycerol from Sigma-Aldrich (purity 99%). Experiments with glycerol must be performed in closed boxes with desiccant, in order to avoid taking up atmospheric water. The solid substrates are oxidized silicon wafers (crystallographic plane 100, p doped, purchased from Siltronix), cleaned by oxygen plasma. The underlying silicon bears a natural oxide layer typically 2 nm thick, of which the properties are similar to those of silica. Although an oxidized 'silicon wafer' is a well defined substrate, this is a complex one, as the interactions between LCs, and silicon or silica, are quite different [11, 12].

2.2. Wettability of the substrates by the cyanobiphenyl LCs [15–27]

- We studied 5CB on wafers some years ago [15–18]. The nematic phase of 5CB wets oxidized silicon wafers[2], while the isotropic phase does not. Therefore, the NI transition coincides with a wetting transition [15–18]. The change in 5CB surface tension at the transition is less than 5×10^{-4} N m^{-1} [2–9].
- On glycerol, it is known that 5CB spreads spontaneously in the nematic range [26, 27]. This is also the case for 6CB and 8CB (both in the nematic and smectic phase) [23–25]. More recently, we have checked that 7CB behaves the same.

[2] Note that anchoring defects may stop the spreading of macroscopic 5CB nematic drops [18] and that smectic defects have a similar effect on macroscopic 8CB drops [28, 29]. In both cases, microscopic droplets spread spontaneously. Note also that nematic 5CB wets silicon but not silica [19].

- On water, it is known that 8CB spreads in the smectic and nematic range [20–23], but data are missing for the lower members of the series. We have observed spreading for the standard 6CB [23–25]. Systematic checks with the 5CB and 7CB have been performed more recently. The standard 7CB sample wets marginally[3]. For standard 5CB, one observes an initial spreading followed by retraction and formation of small droplets after a variable but relatively short time (1–15 min), too short to implicate contamination effects in a well protected set-up. In contrast, the high purity sample (>99%) wets water marginally. In conclusion, 6CB and 8CB wet water, while 5CB and 7CB are close to a wetting transition. For the uneven compounds, the purity of the sample is critical. Let us relate these behaviours to surface tension measurements available in the literature.

2.3. Surface and interfacial tension measurements

The surface tensions of the *n*CB have been measured by many groups. For 5CB at room temperature, values between 40×10^{-3} N m^{-1} [1] and 28×10^{-3} N m^{-1} [2–4] are reported. Such a large scattering of data requires discussion: while the surface tension decreases in the presence of surface active impurities, the measured values are too large if full equilibrium is not reached. This has been used to argue [5–9] against the use of a Wilhelmy plate, as in [1]. Recent experiments use the pendent drop method under inert atmosphere and carefully check the long time stability of the data [5–9]. The results[4] converge around $33–35 \times 10^{-3}$ N m^{-1}.

The surface tension of the next members of the series is lower. From [5], at ambient temperature,

$$\gamma_{5\mathrm{CB/gas}} = 35 \times 10^{-3}\ \mathrm{N\ m^{-1}},$$

$$\gamma_{6\mathrm{CB/gas}} = 32.7 \times 10^{-3}\ \mathrm{N\ m^{-1}},$$

$$\gamma_{7\mathrm{CB/gas}} = 31.7 \times 10^{-3}\ \mathrm{N\ m^{-1}},$$

$$\gamma_{8\mathrm{CB/gas}} = 29.6 \times 10^{-3}\ \mathrm{N\ m^{-1}}.$$

It is difficult to find values of the interfacial tension between *n*CB and another dense phase. We found one for 5CB–water, $\gamma_{5\mathrm{CB-water}} = 26 \times 10^{-3}$ N m^{-1} (with the Wilhelmy plate [1]) and two identical ones for 5CB/glycerol, $\gamma_{5\mathrm{CB-glycerol}} = 16.2 \times 10^{-3}$ N m^{-1} (with the pendent drop method [6, 7]). Interfacial tensions between *n*CB and silicon wafers are not available.

2.4. Discussion and comments

Both surface and interfacial tensions are available only on liquid substrates, and only for the 5CB.

Complete wetting means $S_0 > 0, S = 0$, while initial spreading followed by receding means $S_0 > 0, S < 0$.

- The initial spreading on glycerol and water agrees well with the available data:
  - * on glycerol [1, 5–7]
    $S_0 = 64 - (35 + 16) = +13 \times 10^{-3}$ N m^{-1} [5, 6, 7]
    or $64 - (40 + 16) = +8 \times 10^{-3}$ N m^{-1}
    $[1, 6, 7] > 0$
  - * on water [1]

$$S_0 = 72.8 - (40 + 26) = +6.8 \times 10^{-3}\ \mathrm{N\ m^{-1}} > 0.$$

- At long times, complete wetting is observed on both liquids for the pure 5CB sample, but only on glycerol for the standard one. While the precise value of S is not very meaningful, as it is in any case close to zero, we must point out that the elaborated pendent drop experiments for measuring surface and interfacial tensions in *n*CB have always been performed with standard samples. The presence of a surface active impurity explains that the value ($33–35 \times 10^{-3}$ N m^{-1}) of the surface tension of the standard samples [5–9] is lower than that (40×10^{-3} N m^{-1}) of the pure compound [1]. The difference in the values is due to the purity of the sample and not to the use of a Wilhelmy plate in [1]. A preferential location of the impurity at the air–water interface, increasing the film pressure, explains the change in wetting behaviour. Actually, $S \cong S_0 - \pi$.

As for benzene, further information may be obtained from film pressure measurements, i.e. at the microscopic scale.

3. Specific behaviour at the microscopic scale

3.1. Film pressure measurements

Surface pressure isotherms provide the LC film pressure,

$$\pi = \gamma_{\text{bare liquid substrate–air}} - \gamma_{\text{liquid substrate with film–air}},$$

as a function of the surface area per molecule of LC. Information on the film structure can be extracted. Most studies focus on the low density range, where the film is a monolayer. When density is increased, the isotherm may or may not indicate the presence of multilayers. This is the range of interest of the present study. Equilibrium with the bulk would be reached at higher molecule density.

- Surface pressure isotherms of several *n*CB s on water can be found in the literature [1, 20–22, 31]. Our measurements for 8CB (figure 1), 5CB (figure 2) and 6CB (figure 2, inset) agree with available data. The value of the surface pressure for the compact monolayer is practically the same for the three compounds, around $\pi = 5 \times 10^{-3}$ N m^{-1}. A shoulder revealing a compact trilayer is visible for the 8CB ([20–22] and figure 1) with $\pi \approx 6 \times 10^{-3}$ N m^{-1}. Our data for 6CB show a slight shoulder, but the increase in π is barely 0.2×10^{-3} N m^{-1} (inset in figure 2, no previously published data available). For 5CB, no shoulder is visible ([31] and figure 2), which means that the isotherm provides no information on the

[3] The 7CB must be deposited above 30 °C.

[4] This is a plausible value considering the models of the 5CB molecule at the air interface [10, 30].

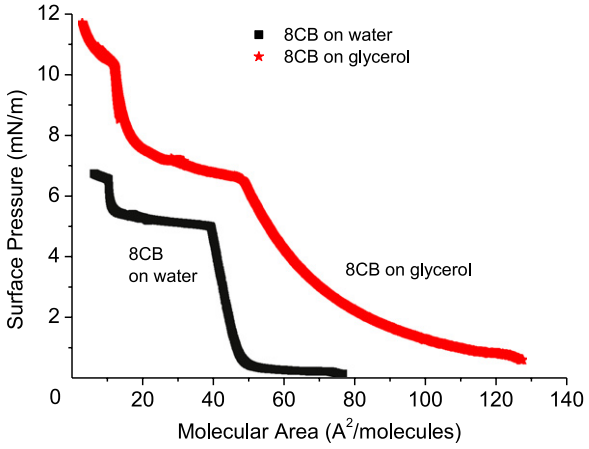

Figure 1. Surface pressure π isotherms of 8CB on water and glycerol at room temperature. The two curves give evidence of well defined monolayer and trilayer structures. A dense monolayer is obtained at a molecular area of $\sim$50 Å^2/molecule and a dense trilayer at $\sim$10 Å^2/molecule. The π values are larger on glycerol, and the isotherms smoother, which suggests that the films are softer. Isotherms were run with a KSV Minimicro trough (initial area 51 mm $\times$ 165 mm) and compressions were run at 1 mm min^{-1} for water and at 0.2 mm min^{-1} for glycerol (humidity: 20–30%).

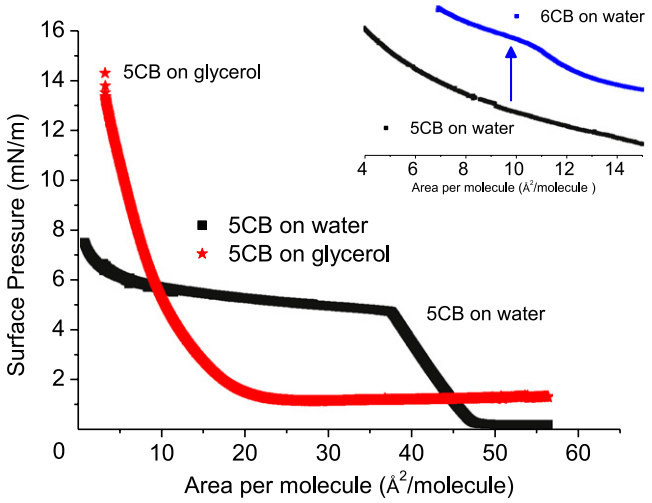

Figure 2. Surface pressure π isotherms of 5CB on water and glycerol at room temperature. On water, no dense trilayer is observed. On glycerol, no dense monolayer is observed. Compressions were run at 1 mm min^{-1} for water and at 0.2 mm min^{-1} for glycerol (humidity: 20–30%) with a KSV Minimicro trough (initial area: 51 mm $\times$ 165 mm). There is no significant change between the pure and standard samples. Inset: the isotherm of 6CB on water is similar to that of the 5CB except around 10 Å^2/molecule. It has been shifted for more visibility. For 6CB a small compression of the trilayer is observed on water.

film structure. The isotherms of pure and standard samples do not differ for surface areas larger than 5 Å^2/molecule. Evidence of the surface active impurity is observed at higher density.

For the pure 5CB sample, the surface pressure stays around 5–6 $\times$ 10^{-3} N m^{-1}; therefore, $S_0 - \pi$ is slightly positive: this means complete wetting and agrees with experiment. The standard sample does not wet: the surface active impurity is present at the air–water interface, and the increase of the film pressure at high compression leads to a negative value of $S_0 - \pi$. The next members of the *n*CB series wet water, which means that $S_0 - \pi$ stays positive despite the presence of impurities.

- Very few film pressure isotherms on glycerol are available in the literature [32, 33], and none with *n*CB. The high viscosity of the subphase requires a very slow displacement of the trough barriers, but with enough care film pressures are actually measurable [32]. For a given compound, the isotherms on glycerol may differ from the ones on water. This is actually the case here, as shown in figures 1 and 2, where the isotherms of 8CB and 5CB are plotted. On glycerol, one cannot even distinguish the 5CB monolayer.

  This is a quite unexpected result: as already mentioned, and as it will be illustrated in the following, the behaviour of *n*CB films on water and glycerol is globally very similar. Why the pressure isotherms are so different is an open question.

3.2. Structure of thin films, and contributions to the surface energy [19, 34–36]

Let us restrict ourselves to the complete wetting case, and consider thin LC films in the bulk nematic range of temperatures, far from the NI transition. Besides surface pressure isotherms on liquid substrates, spatially resolved ellipsometry, Brewster angle microscopy and interferometry provide information on the contributions to the surface free energy. We have studied 5CB and 6CB on silicon wafers, 5CB, 6CB, 7CB and 8CB on glycerol and 6CB, 7CB and 8CB on water.

It is convenient to describe the common general scenario observed in these systems with reference to the shape of 5CB microdroplets spreading on silicon wafers [15–17]. As the spreading is very slow, the drop profile is quasi-stationary and provides information on the free energy in the whole range of thickness.

- A typical drop profile is shown in figure 3 [37]. There is a forbidden range for the film thickness, which corresponds to the vertical part $\alpha\beta$ in the profile. The thinner part of the drop (below α) is layered, i.e. controlled by structural short-range interactions. At room temperature, i.e. far below the NI transition ($T_{NI} \approx 35.3\,^{\circ}$C for the 5CB), the structure at point α is a trilayer of molecules [15, 38]. When the transition is approached, a bilayer forms on top of the trilayer ($T = 28\,^{\circ}$C, figure 3). The structure closer to the transition is not discussed here [39]. The thicker part of the drop (above β) is controlled by the long-range interactions in nematic LCs. *A priori*, usual disjoining pressure terms [34] such as van der Waals and possibly pseudo-Casimir [19] contributions, nematic elastic terms [35] and anchoring energies at interfaces [36] come into play.

  A more recent ellipsometric study of 6CB drops shows the same scenario. At room temperature, α is a trilayer of

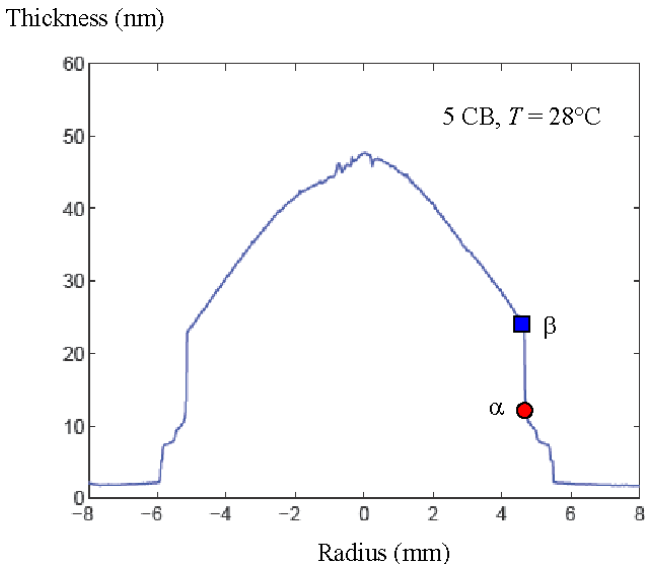

Figure 3. Ellipsometric profile of a 5CB microdroplet on a silicon wafer in the nematic range of temperatures (from [37]). There is a vertical part in the profile between the lower boundary α and the upper boundary β. The baseline is the 2 nm thick silica layer. The lower boundary α is a trilayer of molecules plus a superimposed bilayer. At $T \leqslant 24\,°C$, only the trilayer is present.

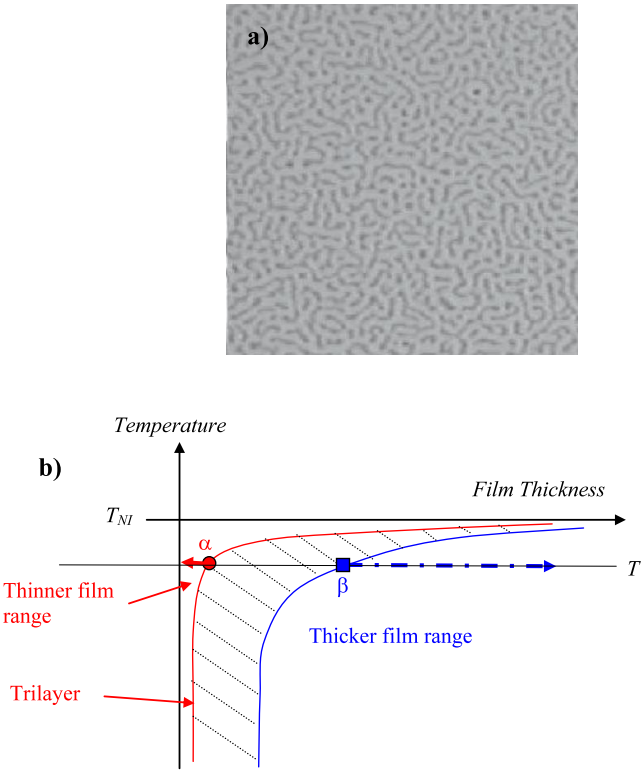

Figure 4. (a) Typical microscope image of a 5CB film with an average thickness between α and β deposited on a silicon wafer in the nematic range of temperatures. White parts correspond to the lower boundary value α, and dark parts to the upper boundary value β from [37]. (b) 'Phase diagram' for the thin LC films in the bulk nematic range of temperature. For deposited films with an average thickness between α and β, only the boundaries α and β are observed at full equilibrium (a). For droplets spreading slowly on solid substrates, the allowed thicknesses are met in both the thinner and thicker film ranges (figure 3). On liquid substrates, metastable situations are the rule and allowed thicknesses other than α and β are observed on flat films.

molecules and the thickness at β is again between 20 and 30 nm [23].

If instead of a drop one prepares a spin-coated sample where the average thickness is between α and β, one observes coexistence between the two thicknesses α and β (figure 4(a), from [37]).

- The scenario on water and glycerol is surprisingly similar to that on wafers; again, whatever the *n*CB, provided complete wetting is achieved, (i) there is a forbidden range for the film thickness, (ii) the boundary α is a trilayer on water and a uneven multilayer on glycerol and (iii) the thickness at the β boundary is between 20 and 30 nm.

  However, two specific behaviours complicate the situation:

  * First, several allowed thicknesses are observed simultaneously, both for the thinner ($\leqslant\alpha$) and the thicker films ($\geqslant\beta$, see the arrows in figure 4(b)). This means that metastable states are the rule.

    The occurrence of metastable states on liquid substrates has been already observed with the smectic phase of 8CB on water [20, 22]. In the present case, the behaviour of the thinner films ($\leqslant\alpha$) is quite similar to that observed at the edge of droplets spreading on silicon wafers (figure 3), i.e. a smectic-like structure controlled by short range structural interactions. However, we do not understand the qualitative difference between the film shapes observed on water (figure 5) or glycerol (figure 6).
  * Second, the thicker films ($\geqslant\beta$) show long wavelength instability patterns (long means much larger than the film thickness); see figure 7. Again, the pictures on glycerol (figure 7(a)) and water (figure 7(b)) look qualitatively different, although the dependence of stripe wavelength on film thickness is quite similar ([23, 24] and figure 7(c)).

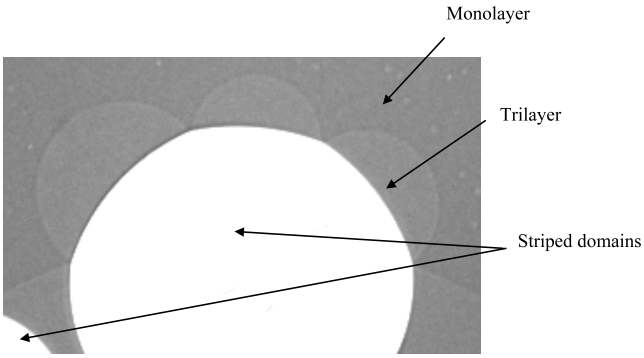

Figure 5. 6CB on water at room temperature. The white parts are striped nematic domains where the camera is saturated. Curved trilayer domains are in contact with them. These trilayer domains are on the other side in contact with a monolayer.

Stripe patterns of 5CB films on glycerol have been studied previously [26, 27]. They are due to perturbations of a distorted

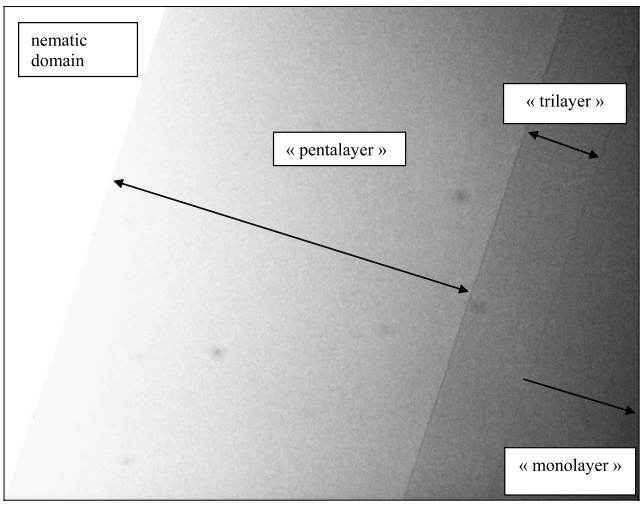

Figure 6. 6CB on glycerol at room temperature. Multilayers exist on glycerol. Note that on glycerol the boundaries are straight lines.

nematic structure, such as the one in figure 8, where the nematic director rotates inside the yz plane with translational symmetry in the xy plane[5]. For all the systems investigated here, the anchoring is planar on the substrate (the nematic director tends to be in the substrate plane) and homeotropic at the free interface (the nematic director tends to be normal to the interface). Therefore, the structure is distorted. If the bulk elastic constants have the same value K, the contributions to the free energy per unit area in a distorted film of thickness h can be written as

$$f = \frac{W_1}{2}\cos^2\theta_1 + \frac{W_2}{2}\sin^2\theta_2 + \frac{K}{2h}(\theta_1 - \theta_2)^2.$$

Here θ_1 is the actual angle of the nematic director with the normal at the substrate (the optimal value is $\pi/2$), θ_2 is the actual angle of the director with the normal at the free surface (the optimal value is zero), and the W_i are the anchoring energies per unit area [36].

Stripe patterns are due to twist oscillations of the nematic director out from the initial yz plane of the figure 8, which efficiently relax the elastic splay–bend energy [26, 27]. Periodic oscillations of the director in the xy plane lead to stripes because the refractive index is modified. The wavelengths are much larger than the film thickness provided the planar anchoring is stronger. This is why they are observable on liquid substrates (the anchoring is stronger on water and glycerol) but not on silicon wafers (the anchoring is stronger on air).

4. Microscopic scale: discussion and open questions

4.1. Distorted nematic structure and β boundary

Stripe patterns are observable on water and glycerol, which proves that the initial film structure is distorted [26, 27]. This proof is quite useful when orders of magnitude are considered. Actually, the simple distorted structure of figure 8 is energetically favourable only if the thickness h is larger than a threshold $h_C = |\frac{K}{W_1} - \frac{K}{W_2}|$ [40]. Thinner films should be

[5] Such a planar distortion is a combination of splay and bend deformations [35].

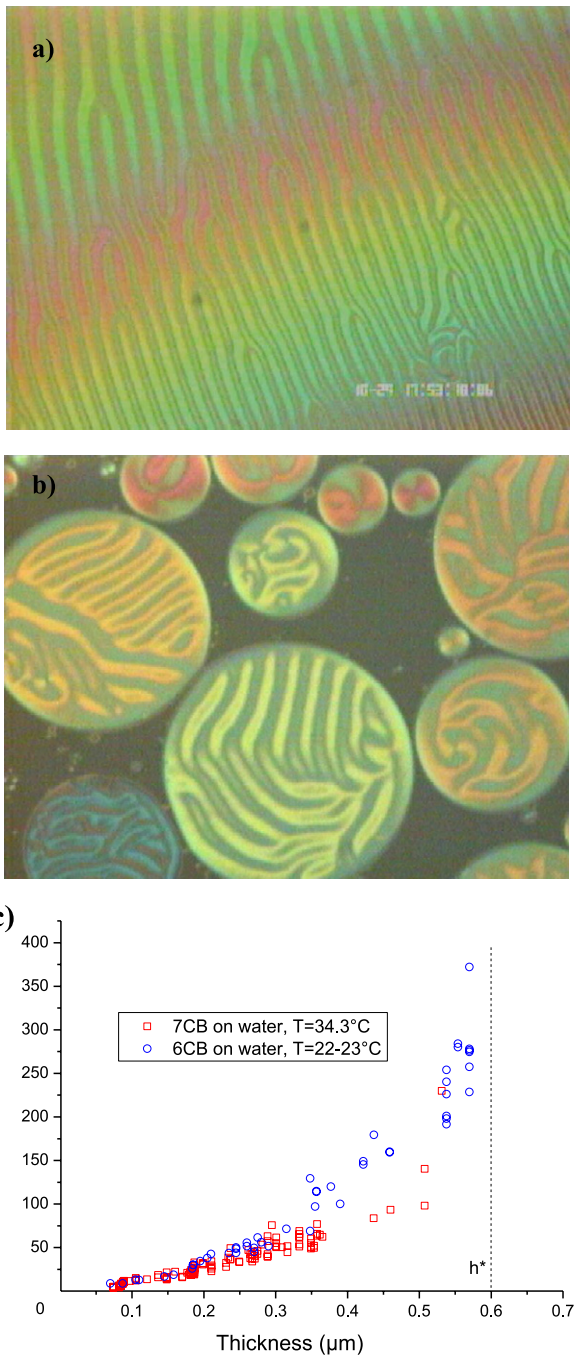

Figure 7. (a) Nematic 8CB on glycerol at 36 °C. A continuous film with variable thickness is obtained. Newton colours allow us to calculate the local film thickness. Continuous flat films are also observable. (b) 6CB on a water substrate: the continuous phase is a trilayer of molecules. Striped flat nematic domains with different colours, i.e. different thicknesses, coexist with it. (c) Wavelength of stripes versus film thickness for 7CB and 6CB in the nematic range. Both series of data are far (7–8 °C) below the nematic–isotropic transition temperature. Wavelengths are much larger than film thickness. For films thicker than $h^* \sim 0.6$ μm, nematic defects replace stripes. h^* is almost the same for 5CB, 6CB and 7CB on water and glycerol. Circles, 6CB; squares, 7CB.

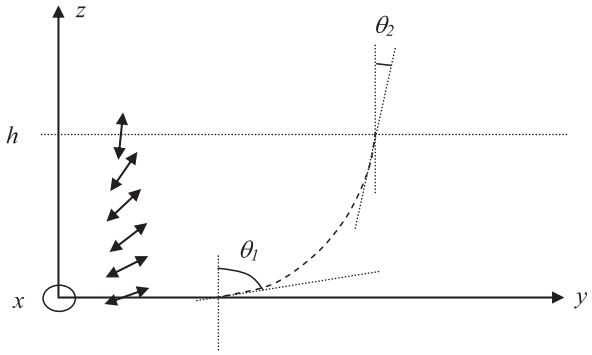

Figure 8. Simple distorted nematic structure, depending only on z. The preferred anchoring is planar and along y at the lower interface, homeotropic at the upper one. The nematic director rotates inside the yz plane. The elastic energy may be reduced if the director is allowed to escape from the yz plane by twist deformation. The simplest instability pattern corresponds to stripes parallel to y [26, 27].

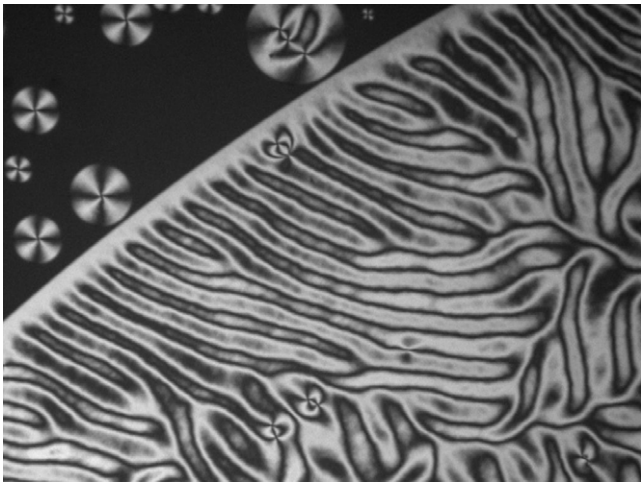

Figure 9. 6CB on water. Edge of a nematic domain. Stripes do not exist at the edge of the domain, where the elastic energy for distortion cannot be relaxed. The configuration becomes a planar one.

homogeneous, with the director parallel to the direction of the stronger anchoring, i.e. fully planar on water and glycerol, and fully homeotropic on wafers[6]. While accepted values for h_C are around 0.2–0.3 μm [25], striped films are observed at much lower thicknesses, till the β boundary, i.e. 20–30 nm. This apparent inconsistency has been explained by Sparavigna *et al* [27]: the threshold between distorted and planar configurations is h_C only in the absence of twist deformation. If twist is allowed, the threshold thickness decreases. One may expect the structure of striped films much thinner than h_C to be strongly modified with respect to the simple distorted configuration.

In principle, all the tools for a complete description of the *n*CB films on wafers, water and glycerol are available. In fact, the resolution of the equations is still to be done [41–45]. The work by Sparavigna concerns only the vicinity of the planar–stripes transition [27]. On the other hand, the pioneering model by Lavrentovich and Pergamenshchik (LP) [26, 41–43], which describes the dependence of the stripe wavelength on the film thickness in the 5CB/glycerol case, is a first order perturbation of the distorted state of figure 8 and does not account for stripes in films thinner than h_C. In fact, no model for the very thin film range is available yet. Note that the LP model also meets difficulties at the upper thickness threshold of the stripe patterns (see figure 7(c)), as it requires very precise ratios of elastic and anchoring constants [26]. Our data provide similar upper thresholds for 5CB, 6CB and 7CB on glycerol, and 6CB and 7CB on water, which excludes such a constraint.

4.2. Specificities of water and glycerol

Let us now comment on the difference between water and glycerol as the liquid subphase.

- For the thinner films ($\leqslant\alpha$) far from the NI transition, microscope observations suggest that uneven multilayers with different thicknesses exist on glycerol in the thinner film range, while only monolayers and trilayers are allowed on water.

  We have no explanation for such behaviour. As previously mentioned, film pressure isotherms provide no information. Molecular modelling might be useful.
- In the thicker film range, and whatever the LC (5CB, 6CB, 7CB, 8CB), isolated flat domains are the rule on water, while continuous films with thickness gradients are easily obtained on glycerol.

  The explanation may be that thickness gradients remove the planar degeneracy on liquid substrates. They introduce a preferred orientation for the nematic director, i.e. an 'effective azimuthal' anchoring, as discussed in [27, 45]. This anchoring reduces the ability of the system to undergo twist deformations, i.e. the possibility for the film to relax the distortion energy [27]. We assume that this azimuthal anchoring is larger on water, which is not able to accommodate thickness gradients for films significantly thinner than h_C.

5. Line tension in the 6CB–water system

5.1. Static behaviour

A consequence of azimuthal anchoring is that the edge of a nematic domain cannot be twisted and so cannot accommodate stripes. This is actually observed on water: instabilities disappear in the vicinity of the edge, where a planar structure is visible (figure 9). A measurable line tension τ is associated with this conflicting boundary. The line tension has been studied for 6CB on water [25].

The excess energy at the edge of the 6CB nematic domains on water increases linearly with thickness up to 0.2 μm [25] and is responsible for their circular shape in the final metastable state (figure 7(b)).

[6] Such a homeotropic structure has been proposed on silicon wafers [19], in which case the repulsive pseudo-Casimir interaction due to the fluctuations of the nematic director orientation would replace the elastic contribution [35]. However, the pseudo-Casimir force scales as h_C^{-3} and is fully negligible with the actual values $h_C \sim 0.2$–0.3 μm.

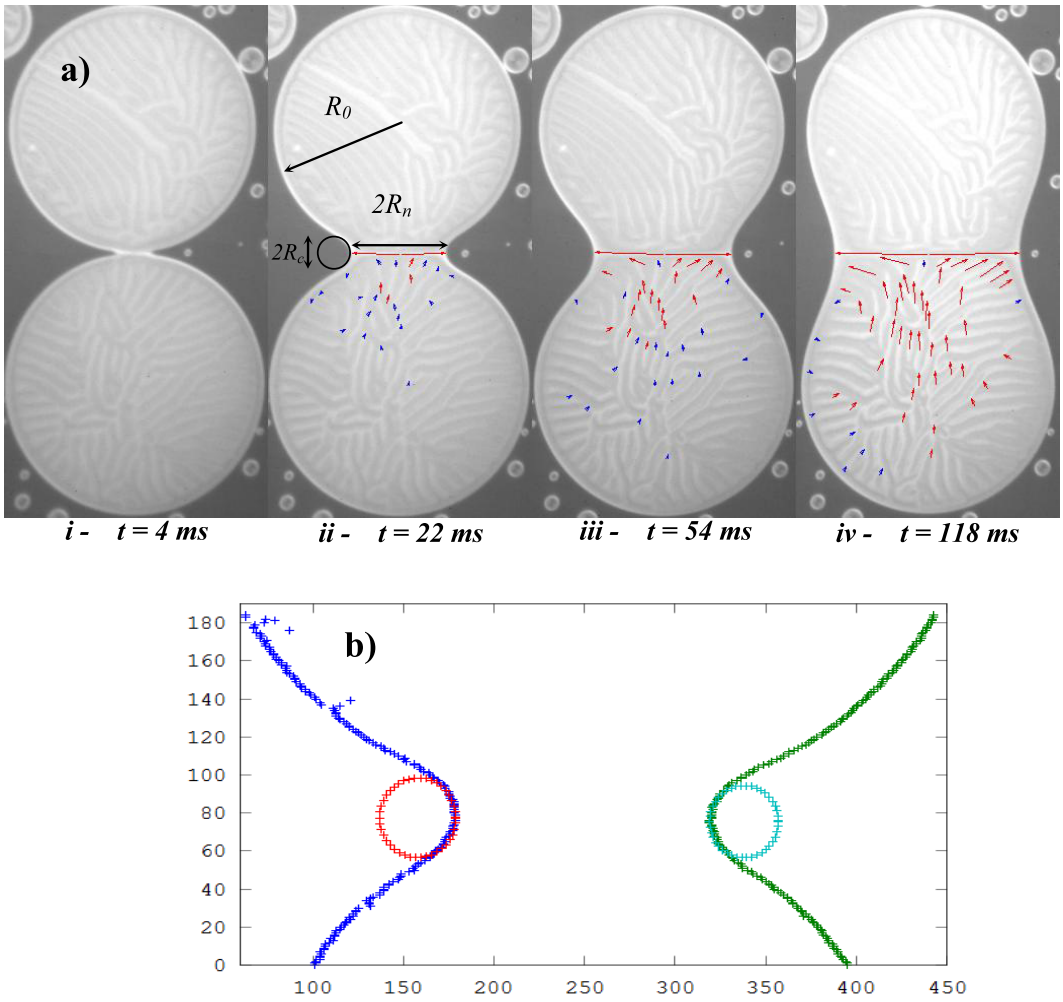

Figure 10. (a) Image sequence of a coalescence between two domains with the same thickness and the same initial radius R_0. The time t after the initial contact between the domains ($t = 0$) is indicated at the bottom. Arrows indicate the direction and the value of the displacement dr at selected points between their position at $t = 0$ and their position at t. Therefore we can visualize the flow inside the domains. Size of images: 219 μm $\times$ 506 μm. Long red arrows are for displacements $dr > 6$ μm. Short blue arrows are for displacements 6 μm $> dr >$ 2.5 μm. Threshold values 6 and 2.5 μm are arbitrary values taken in the image analysis. Similar arrow patterns are obtained for other threshold values. Displacements lower than 2.5 μm were attributed to uncertainty in the positioning of the selected points. (b) Typical image analysis of the profile during coalescence and calculation of the curvature radii on the right $R_{c-right}$ and the left R_{c-left} side of the neck region. Length scales are in micrometres on both axes. Performed with Image J and Octave.

5.2. *Dynamic behaviour*

- *Line tension driven coalescence process.* The occurrence of a line tension has interesting consequences on the dynamics of the system. Indeed, after film deposition and complete evaporation of the solvent, coalescence between nematic pancakes may take place. This is a 2D process, as the radius of the domains is much larger than their thickness. A typical sequence of coalescence between two domains with the same thickness h and same radius R_0 is shown in figure 10(a). The contact produces at early times a 'neck' of half-width R_n (referred to as 'neck radius' in the following, even if it is not a 'radius' in 2D), which increases with time and disappears when the curvature of the final pancake becomes positive everywhere.

  * In contrast to most of the studies on coalescence, here the dynamics is governed by the line tension τ between the nematic domains and the trilayer phase and not by the surface tension.
  * At the end of the coalescence process, when the neck has disappeared, the surface dissipation can be neglected and bulk dissipation is dominant [22, 25, 48, 52]. A theoretical treatment by Stone *et al* [48] describes the relaxation of an elliptical towards a circular shape. This relaxation is exponential with a characteristic time

$$T_c \approx \frac{\eta_b R_f^2}{\tau}.$$

  It depends on the final radius R_f, on the line tension τ and on the bulk viscosity η_b of the subphase. This has been used to measure the line tension [22, 25, 52]. Here we want to investigate the early stages of the coalescence process, i.e. the short time dynamics of a

2D[7] coalescence driven by line tension. This situation has not been addressed before.

- *Previous studies on early steps of coalescence.* Previous studies of the early steps of the coalescence mainly deal with classic 3D droplets where just after the contact the dynamics is driven by the capillary forces. In 3D, an initial viscous regime takes place where the neck radius increases linearly with time [49]. This has been checked for numerous systems. Alkane lenses on water [51] are relatively thick (the contact angle is larger than 40° for dodecane) and the dynamics is similar to 3D systems. This is not the case here.
- Specificity of our system
  * As the coalescing domains are nematic phases, we must first investigate the role of the nematic elasticity. An easy way is to observe the location of the stripes during the process, which allows us to visualize the flow[8]. We have analysed the displacement of selected points in the stripe pattern during the coalescence in figure 10(a). Arrows indicate the displacement of the stripes from their original position. It is clear that the flow is mainly localized close to the neck and that the displacement inside the nematic pancake is much slower than the displacement at the neck. Furthermore, most stripes do not move at all. This supports the idea that the nematic elasticity does not play a significant role in the early steps of coalescence[9].
  * Hence, the coalescence is governed by pure hydrodynamics. The corresponding Navier–Stokes equations can be found in [52]. Below we merely identify the leading terms.

5.3. Leading terms in early steps of 2D coalescence

- Let us identify the driving term and the characteristic length scales.
  * Here, the coalescence occurs between two pancakes with the same radius R_0 (figure 10(a)). The leading driving term is the gradient of surface pressure between the neck region N and the inner part I of the nematic domain. Let R_c be the curvature radius at the neck. The Laplace law in 2D gives

$$\pi_N - \pi_{trilayer} \approx -\frac{\tau}{R_c} < 0 \qquad \pi_I - \pi_{trilayer} \approx \frac{\tau}{R_0}.$$

At short times R_c is much smaller than R_0. Therefore,

$$\pi_N - \pi_I \approx -\frac{\tau}{R_c}.$$

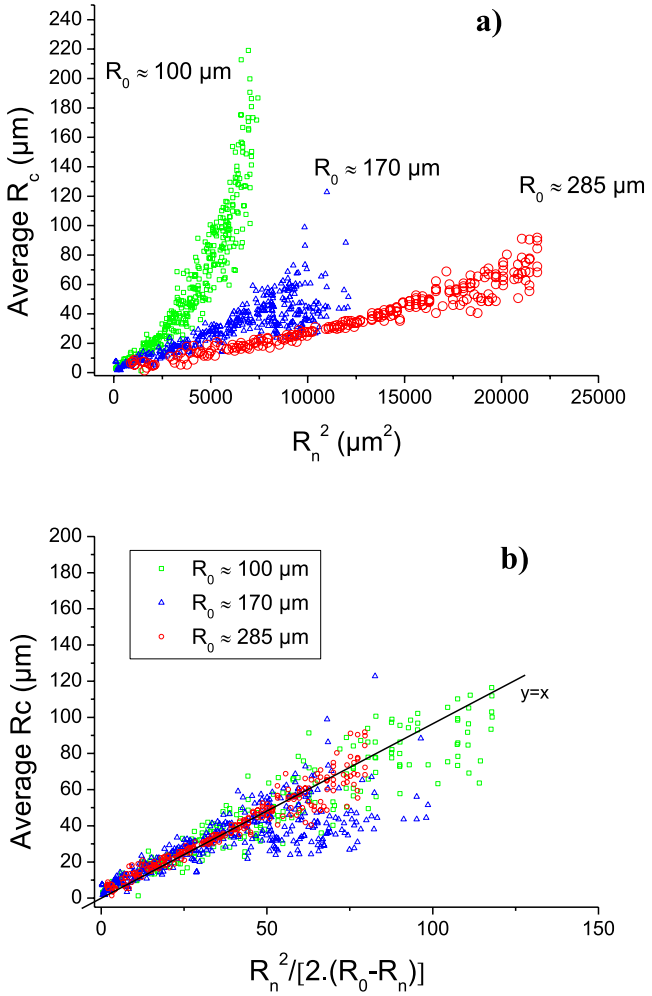

Figure 11. (a) R_c versus R_n^2. Average radius of curvature R_c versus the square of neck radius R_n for three coalescence processes. Values of R_0 are indicated on the curves. Standard image analysis using Image J and Octave was performed to calculate the radius of curvature on the left R_{c-left} and on the right side $R_{c-right}$ on the neck region (see figure 10(b)). Data points represent the average. (b) Rescaling of the curves with R_0—the nematic domain radius. A fairly good collapse is obtained within the uncertainty of the calculation method.

  * By simple geometric argument, we expect $R_c \approx \frac{R_n^2}{2(R_0-R_n)}$, a relation which can be easily checked all along the coalescence process thanks to image analysis (figure 11(a)). An example of such an analysis is shown in figure 10(b). The results show that the relation is obeyed (figure 11(b)). Therefore, at the beginning of the coalescence process, when $R_n \ll R_0$, one has

$$\pi_N - \pi_I \approx -\frac{\tau}{R_c} \propto -\frac{\tau R_0}{R_n^2}.$$

This formula provides the combination of characteristic lengths involved in the driving term.

- The next step is to identify the dominant dissipation process. Both surface and bulk viscous dissipation can occur. At the end of the coalescence, it is known that bulk

[7] A few studies have already dealt with 2D coalescence [46, 47]. In thin copolymer films on a solid substrate [46], the dynamics is very slow (several hours) and seems to be controlled by diffusion. In the case of free stratifying foam films [47], only the late stage of relaxation at the end of the coalescence was studied.

[8] This is more difficult in 3D studies.

[9] Note that a reorganization of the stripe pattern may occur at the very end of the coalescence process, especially when the domains do not have the same thickness (not shown here).

dissipation dominates, because the characteristic length scale is the radius R_f of the final droplet [22, 25, 48, 52]. In the earliest stage of the coalescence, the question is open.

* The dynamics of the neck radius R_n is shown on figure 12, and does not obey any simple power law. Noticeably, the linear dependence $R_n \propto (\gamma t/\eta)$ observed in the case of 3D coalescence of droplets with viscosity η and surface tension γ [49] has no counterpart here. Hopper has theoretically treated the 2D coalescence for liquids with viscosity η and surface tension γ [54]. Considering the coalescence between two infinitely long viscous cylinders of initial radii R in an inviscid medium (non-viscous), Hopper showed that the neck radius R_n in a cross section obeys [54]

$$R_n \propto -(\gamma t/\eta)\ln(\gamma t/\eta R).$$

  If we replace the surface tension γ by the line tension τ and the viscosity η of the cylinders by the surface viscosity η_s of the nematic pancake [52], we can fit the beginning of the coalescence process using as typical surface viscosity $\eta_s \approx \eta_{LC} h \approx 10^{-8}$ Pa s m, where η_{LC} is the bulk viscosity of the LC [47, 53]. This suggests that the process is driven by surface dissipation in the pancake at very short times.
* However, the Hopper's formula does not take into account the viscosity of the surrounding—i.e. trilayer—phase. When the outer fluid is viscous, Eggers *et al* [50] have shown that the 3D dynamics is similar but a bubble of the exterior fluid is caught in the neck region. No such bubble develops during the coalescence of our nematic pancakes (6CB on water, far below the NI transition), which seems to indicate that the surface viscosity of the trilayer is much lower than the surface viscosity of the nematic domain. This validates our approach at short times.
* A global model is needed which must take into account the transition between surface and bulk dissipation. This will be addressed in the near future.

6. General conclusion

- The wetting behaviour of the cyanobiphenyl series (5CB–8CB) has been investigated on different substrates (oxidized silicon wafers, water and glycerol). As a rule, the nematic phase of these LC wets the substrates, although marginally on water, where the purity of the samples is critical.
- Globally, very similar behaviours are observed at the microscopic scale: far from the NI transition, molecular films controlled by short-range interaction coexist with mesoscopic films mainly controlled by nematic elasticity and anchoring terms. There is a forbidden range of thickness which is practically the same (2–5 to 20–30 nm) whatever the LC and the substrate. The theoretical tools able to account for these behaviours are identified [26, 27, 41–45, 55], even if explicit formulae are not available yet.

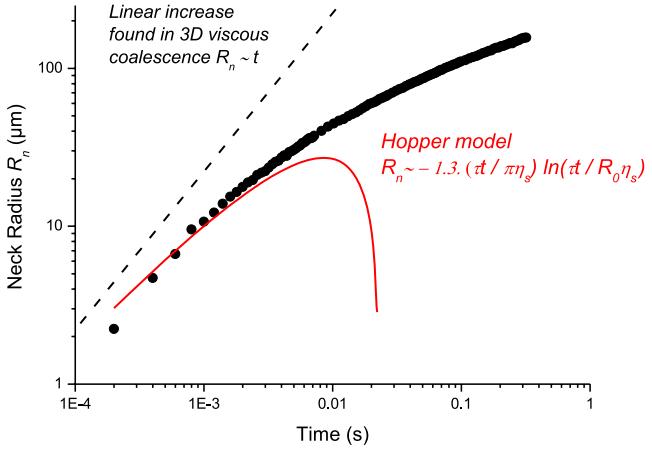

Figure 12. Evolution of the neck radius as a function of time: R_n (μm) versus time (s). Circles: example of coalescence driven by line tension (experimental data points). Line: Hopper model. Dashed line: the usual viscous regime when surface tension is the control parameter in 3D is characterized by a linear increase ($R_n \approx (\gamma/\eta)t$). $R_0 \cong 170$ μm, pancake thickness $h \cong 0.11$ μm and $\tau \cong 74$ pN estimated from [25].

- More specifically, and counter-intuitively, the structure of mesoscopic and molecular films on water and glycerol might significantly differ. Extended mesoscopic nematic films are obtained on glycerol whereas finite size domains exist on water. Considering molecular films, a dense monolayer phase is well defined on water for 8CB and 5CB, and also on glycerol with 8CB, but it is not possible to observe it for 5CB.
- On water, well defined line tensions between nematic film and trilayer and between trilayer and monolayer can be measured. This is not yet clear in the glycerol subphase. In the last part of the paper, we investigate the dynamics of coalescence between nematic domains of 6CB on water. As no theoretical description is currently available for this line tension driven 2D process, our aim is to identify the leading parameters of the coalescence. At short times the process is governed by surface viscous dissipation, but the transition towards longer times, where the bulk viscous dissipation comes into play, has not been described yet.

Acknowledgment

The present work is supported by the ANR 'DYNINSTA-MOBI' of the French CNRS.

References

[1] Proust J E, Perez E and Ter Minassian L 1978 *Colloid Polym. Sci.* **256** 666
[2] Ganon G J and Faber T E 1978 *Phil. Mag.* **37** 117
[3] Krishnaswamy S 1980 *Proc. Int. Liquid Crystal Conf. (Bangalore, 1979)* ed S Chandrasekhar (London: Heyden) p 487
[4] Korjenevsky V A and Tomilin M G 1993 *Liq. Cryst.* **15** 643
[5] Tintaru M, Moldovan R, Beica T and Frunza S 2001 *Liq. Cryst.* **28** 793
[6] Beica T, Moldovan R, Zgura I and Frunza S 2006 *Proc. Rom. Acad. Ser.* A **7** 1
[7] Tarakhan L M 2006 *Ukr. J. Phys.* **51** 22

[8] Song B and Springer J 1997 *Mol. Cryst. Liq. Cryst.* **293** 39
[9] Song B and Springer J 1997 *Mol. Cryst. Liq. Cryst.* **307** 69
[10] Mach P, Huang C C, Stoebe T, Wedell E D, Nguyen T, de Jeu W H, Guittard F, Naciri J, Shashidhar R, Clark N, Jiang I M, Kao F J, Liu H and Nohira H 1998 *Langmuir* **14** 4330
[11] Churaev N V 1988 *Rev. Phys. Appl.* **23** 975
[12] Adamson A W 1990 *Physical Chemistry of Surfaces* 5th edn (New York: Wiley) and references therein
Bartell F E, Case L O and Brown H 1933 *J. Am. Chem. Soc.* **55** 2769
Harkins W D and Humphery E C 1916 *J. Am. Chem. Soc.* **38** 236
Cassel H 1932 *Trans. Faraday Soc.* **28** 177
[13] Zisman W A 1964 *Adv. Chem. Ser.* **43** 1
[14] de Gennes P G 1985 *Rev. Mod. Phys.* **57** 827
[15] Valignat M P, Villette S, Li J, Barberi R, Bartolino R, Dubois-Violette E and Cazabat A M 1996 *Phys. Rev. Lett.* **77** 1994
[16] Vandenbrouck F, Bardon S, Valignat M P and Cazabat A M 1998 *Phys. Rev. Lett.* **81** 610
[17] Vandenbrouck F, Valignat M P and Cazabat A M 1999 *Phys. Rev. Lett.* **82** 2693
[18] Poulard C and Cazabat A M 2005 *Langmuir* **21** 6270
[19] Ziherl P R, Podgornik R and Zumer S 2000 *Phys. Rev. Lett.* **84** 1228
[20] de Mul M N G and Mann J A 1994 *Langmuir* **10** 2311
de Mul M N G and Mann J A 1998 *Langmuir* **14** 2455
[21] Laüger J, Robertson C R, Frank C W and Fuller G G 1996 *Langmuir* **12** 5630
[22] Zou L, Wang J, Basnet P and Mann E K 2007 *Phys. Rev.* E **76** 031602
[23] Delabre U, Richard C, Guéna G, Meunier J and Cazabat A M 2008 *Langmuir* **24** 3998
[24] Delabre U, Richard C and Cazabat A M 2009 *J. Phys. Chem.* B **113** 3647
[25] Delabre U, Richard C, Meunier J and Cazabat A M 2008 *Europhys. Lett.* **83** 66004
[26] Lavrentovich O D and Pergamenshchik V M 1994 *Phys. Rev. Lett.* **73** 979
[27] Sparavigna A, Lavrentovich O D and Strigazzi A 1994 *Phys. Rev.* E **49** 1344
[28] Bénichou O, Cachile M, Cazabat A M, Poulard C, Valignat M P, Vandenbrouck F and Van Effenterre D 2003 *Adv. Colloid Interface Sci.* **100** 381
[29] Van Effenterre D 1999 *Les Houches Workshop (Oct. 1999)*
[30] Leadbetter A J, Richardson R M and Colling C N 1975 *J. Physique* **36** C1-37
[31] Inglot K, Martynski T and Bauman D 2006 *Liq. Cryst.* **33** 855
[32] Barraud A, Leloup J and Lesieur P 1985 *Thin Solid Films* **133** 113
[33] Nakamura T *et al* 1986 *Chem. Lett.* **15** 709
[34] Derjaguin B V and Landau L D 1941 *Acta Physicochem. URSS* **14** 633
[35] Frank F C 1958 *Discuss. Faraday Soc.* **25** 19
[36] Rapini A and Papoular M 1969 *J. Physique* **30** C4
[37] Vandenbrouck F 2001 *PhD Thesis* University Pierre et Marie Curie, Paris available on line thèses-EN-ligne (CNRS).
[38] Bardon S, Ober R, Valignat M P, Vandenbrouck F, Cazabat A M and Daillant J 1999 *Phys. Rev.* E **59** 6808
[39] Van Effenterre D, Ober R, Valignat M P and Cazabat A M 2001 *Phys. Rev. Lett.* **87** 125701
[40] Barbero G and Barberi R 1983 *J. Physique* **44** 609
[41] Pergamenshchik V M 1993 *Phys. Rev.* E **47** 1881
[42] Lavrentovich O D and Pergamenshchik V M 1995 *Int. J. Mod. Phys.* B **9** 2389
[43] Pergamenshchik V M 2000 *Phys. Rev.* E **61** 3936
[44] Barbero G, Lelidis I and Zvezdin A K 2003 *Phys. Rev.* E **67** 061710
[45] Lavrentovich O D 1992 *Phys. Rev.* A **46** R722
[46] Berger L, Raghunathan V A, Launay C, Ausséré D and Gallot Y 1998 *Eur. Phys. J.* B **2** 93
[47] Heinig P and Langevin D 2005 *Eur. Phys. J.* E **18** 483
[48] Stone H A and McConnell H M 1995 *Proc. R. Soc.* A **448** 97
[49] Yao W, Maris J, Pennington P and Seidel G 2005 *Phys. Rev.* E **71** 016309
[50] Eggers J, Lister J R and Stone H A 1999 *J. Fluid Mech.* **401** 293
[51] Burton J C and Taborek P 2007 *Phys. Rev. Lett.* **98** 224502
[52] Mann E K, Hénon S, Langevin D, Meunier J and Léger L 1995 *Phys. Rev.* E **51** 5708
[53] Schwartz D K, Knobler C M and Bruinsma R 1994 *Phys. Rev. Lett.* **73** 2841
[54] Hopper R W 1990 *J. Fluid Mech.* **213** 349
[55] Barbero G, Dahl I and Komitov L 2009 *J. Chem. Phys.* **130** 174902